

Kent Academic Repository

Full text document (pdf)

Citation for published version

Giovaninni, Giorgia and Moore, Colin J. and Hall, Andrew J. and Byrne, Hugh J. and Gubala, Vladimir (2018) pH-Dependent silica nanoparticle dissolution and cargo release. *Colloids and Surfaces B: Biointerfaces*, 169 . pp. 242-248. ISSN 0927-7765.

DOI

<https://doi.org/10.1016/j.colsurfb.2018.04.064>

Link to record in KAR

<http://kar.kent.ac.uk/67094/>

Document Version

Author's Accepted Manuscript

Copyright & reuse

Content in the Kent Academic Repository is made available for research purposes. Unless otherwise stated all content is protected by copyright and in the absence of an open licence (eg Creative Commons), permissions for further reuse of content should be sought from the publisher, author or other copyright holder.

Versions of research

The version in the Kent Academic Repository may differ from the final published version.

Users are advised to check <http://kar.kent.ac.uk> for the status of the paper. **Users should always cite the published version of record.**

Enquiries

For any further enquiries regarding the licence status of this document, please contact:

researchsupport@kent.ac.uk

If you believe this document infringes copyright then please contact the KAR admin team with the take-down information provided at <http://kar.kent.ac.uk/contact.html>

pH-Dependent Silica Nanoparticle Dissolution and Cargo Release

Giorgia Giovaninni,^a Colin J. Moore,^{b‡*} Andrew J. Hall,^a Hugh J. Byrne,^b Vladimir Gubala^a

^aMedway School of Pharmacy, University of Kent, Central Ave, Chatham Maritime, Kent, ME4 4TB, United Kingdom

^bFOCAS Research Institute, Dublin Institute of Technology, Kevin St., Dublin 8, Ireland

Email: gg238@kent.ac.uk, colin.moore@dit.ie, a.hall@kent.ac.uk, hugh.byrne@dit.ie, v.gubala@kent.ac.uk

*Corresponding author: colin.moore@dit.ie , Tel: +353 1 4027902 , Fax: +353 1 4027901

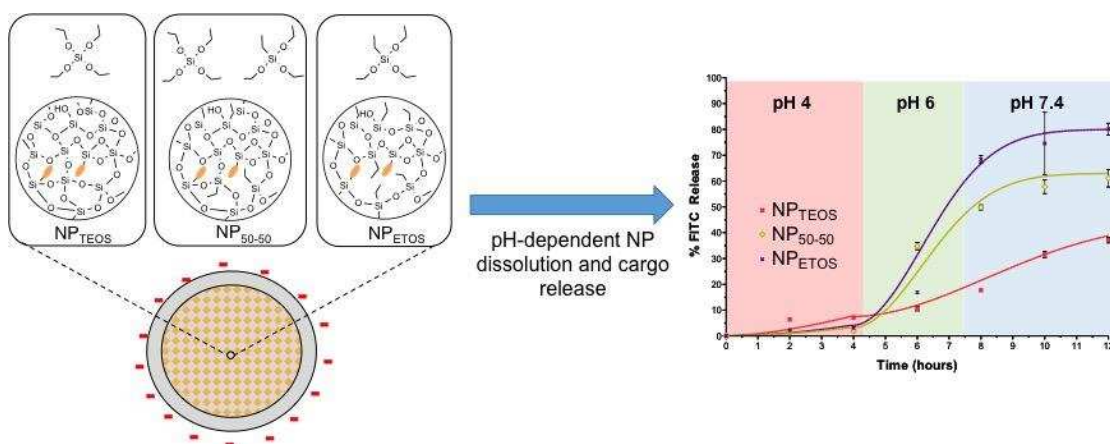
‡Current address: EA 6295 Nanomedicine and Nanoprobes, Faculty of Pharmacy, University of Tours, 31 avenue Monge, Tours 37200, France

30 **Abstract**

31 The dissolution of microporous silica nanoparticles (NP) in aqueous environments of different
32 biologically relevant pH was studied in order to assess their potential as drug delivery vehicles.
33 Silica NPs, loaded with fluorescein, were prepared using different organosilane precursors
34 (tetraethoxysilane, ethyl triethoxysilane or a 1:1 molar ratio of both) and NP dissolution was
35 evaluated in aqueous conditions at pH 4, pH 6 and pH 7.4. These conditions correspond to
36 the acidity of the intracellular environment (late endosome, early endosome, cytosol
37 respectively) and gastrointestinal tract ('fed' stomach, duodenum and jejunum respectively).
38 All NPs degraded at pH 6 and pH 7.4, while no dissolution was observed at pH 4. NP dissolution
39 could be clearly visualised as mesoporous hollows and surface defects using electron
40 microscopy, and was supported by UV-Vis, fluorimetry and DLS data. The dissolution profiles
41 of the NPs are particularly suited to the requirements of oral drug delivery, whereby NPs must
42 resist degradation in the harsh acidic conditions of the stomach (pH 4), but dissolve and
43 release their cargo in the small intestine (pH 6 - 7.4). Particle cores made solely of ethyl
44 triethoxysilane exhibited a 'burst release' of encapsulated fluorescein at pH 6 and pH 7.4,
45 whereas NPs synthesised with tetraethoxysilane released fluorescein in a more sustained
46 fashion. Thus, by varying the organosilane precursor used in NP formation, it is possible to
47 modify particle dissolution rates and tune the release profile of encapsulated fluorescein. The
48 flexible synthesis afforded by silica NPs to achieve pH-responsive dissolution therefore makes
49 this class of nanomaterial an adaptable platform that may be well suited to oral delivery
50 applications.

51 **Graphical Abstract**

52
53
54



55 **Introduction**

56

57 Nanoparticle (NP)-based delivery systems have come to prominence over the past two
58 decades as they can be designed to carry poorly soluble drugs or molecules that are
59 prone to degradation in biological conditions.¹⁻⁴ NPs can also transport therapeutics
60 across highly regulated biological boundaries such as the blood brain barrier.^{5,6} In
61 particular, silica NPs (SiNPs) are regularly described as excellent candidates for drug
62 delivery applications because they are regarded as biocompatible⁷⁻⁹ and inert.¹⁰
63 However, it is the adaptable and flexible nature of siloxane chemistry that makes this
64 class of nanomaterial so widely studied as a drug delivery agent. This is facilitated, in
65 part, by the large number of commercially available organosiloxane derivatives that
66 can be used as precursors for SiNP synthesis. The chemistries of these precursors can
67 vary widely and means that SiNPs can exhibit a range of useful physicochemical
68 properties (e.g. different porosity, charge, hydrophobicity), which, in turn, allows for
69 different kinds of therapeutics to be encapsulated and delivered to disease sites.

Most silica-based drug delivery studies employ mesoporous silica, having pore

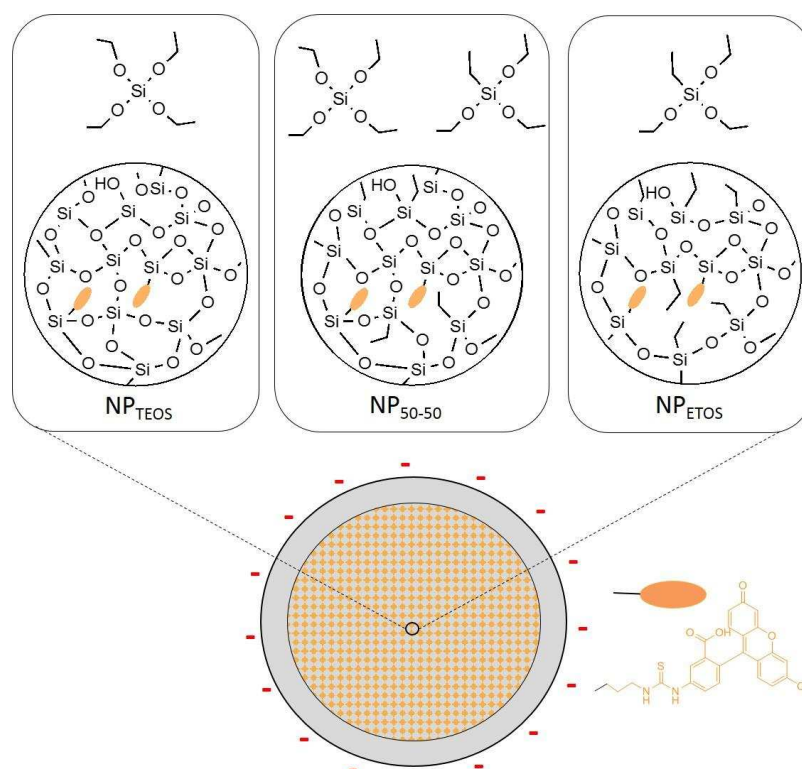


Figure 1: Silica NPs were prepared with different core chemistries by employing different NP precursors during synthesis: tetraethoxysilane (TEOS) or ethyl triethoxysilane (ETOS). These NPs were called NP_{TEOS} and NP_{ETOS}. TEOS and ETOS were also added in an equal molar ratio (NP₅₀₋₅₀). Covalently binding fluorescein (FITC) in the NP cores also provided information about particle degradation and cargo release.

71 sizes of the order 2-50nm, and rely on tunable cargo release via a ‘gatekeeper’
 72 strategy.^{8,11-14} Despite their popularity, the requirement to load cargo and incorporate
 73 gatekeepers after NP synthesis introduces additional complexity to particle design. On
 74 the other hand, microporous silica NPs have characteristic pores of less than 2nm¹⁵,
 75 that are challenging to characterise accurately with appropriate methods and
 76 expertise compared to mesoporous silica.¹⁶ Encapsulataion of different therapeutics
 77 can be achieved during NP synthesis^{2,17,18} and the release mechanism is via the natural
 78 degradation of the silica.¹⁹ The process of NP degradation is therefore largely governed
 79 by the organosiloxane precursors, and their associated physicochemical properties,
 80 that can be easily imparted during synthesis. However, microporous silica remains
 81 understudied as a drug delivery candidate and is more frequently reported in
 82 immunoassays²⁰⁻²² and bioimaging.^{9,23-25} This is surprising, considering the adaptable
 83 nature of silica and the fact that it, in comparison to its mesoporous counterpart,
 84 avoids the need for gatekeeping to control drug release and the associated
 85 complications related to cargo leeching. We therefore feel microporous silica NPs are

86 an interesting nanomaterial to study and have the potential to impact the drug delivery
87 field.

88 We hypothesise the development of a dissolution-based method of controllably
89 releasing encapsulated cargo from microporous SiNPs by synthesising colloids using
90 different organosiloxane precursors. SiNPs are formed utilising hydrolysis but this pH-
91 dependent mechanism is reversible and suggests SiNPs may degrade at different rates
92 in different acidic conditions.

93 Intracellular NP-drug delivery typically requires endocytosis of the nanocarrier
94 to transport a therapeutic across the cell membrane. Trafficking of the NPs from the
95 extracellular environment (pH 7.4) into early endosomes (pH 6) and then to late
96 endosomes/lysosomes (pH 4) means environments of different acidity are
97 experienced. The same can be said for oral drug delivery applications in which
98 medicines first encounter the harsh environment of the stomach (pH 4 in 'fed state')
99 and are then passed to the duodenum (pH 6) and jejunum (pH 7.4) for adsorption.

100 We have synthesised core-shell SiNPs via the reverse microemulsion method
101 (Figure 1) and investigated their dissolution in aqueous conditions at biologically
102 relevant pH (pH 4, pH 6, pH 7.4), similarly to other NP dissolution studies.²⁶⁻²⁹ Different
103 siloxane precursors were employed during the core formation in order to produce
104 particles that exhibit varying degrees of hydrophobicity, which in turn may be able to
105 affect NP dissolution and the ability to host different cargos. A shell composed of
106 tetraethoxysilane (TEOS) and negatively charged phosphonates was then added to
107 each set of particles to insure similar surface chemistry.

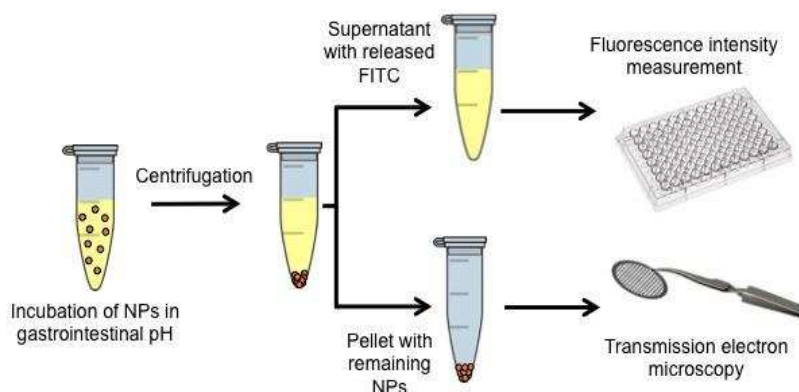


Figure 2: NPs were synthesised using tetraethoxysilane (NP_{TEOS}), ethyl triethoxysilane (NP_{ETOS}) or equal ratio of both (NP_{50-50}), and were degraded in biologically relevant pH. Dissolution of the NPs was assessed by fluorimetry (FITC release from the NPs) and electron microscopy (NP morphology and integrity).

108 The precursors used for core formation were TEOS, ethyl triethoxysilane (ETOS),
 109 bis(triethoxysilyl)benzene and bis(triethoxysilyl)biphenyl. However, the colloids formed
 110 using the aromatic oxysilanes were unstable in aqueous conditions and only particles
 111 formed using TEOS and ETOS were studied to assess dissolution. Degradation and
 112 release of the encapsulated cargo (i.e. fluorescein; FITC) from the SiNPs were
 113 monitored by electron microscopy and fluorimetry (Figure 2), and stability studies
 114 were carried out using dynamic light scattering (DLS). Overall, negligible dissolution
 115 was observed at pH 4 and suggested the NPs may survive the acidic conditions of the
 116 stomach or cellular lysosome, thus minimising cargo release. NP degradation was
 117 accelerated in pH 6 and pH 7.4 and may support the release the encapsulated cargo in
 118 small intestinal pH, at physiological pH or in early endosomes. A study mimicking
 119 progress through the GI tract (i.e. pH 4 to pH6 to pH 7.4) then showed the NPs released
 120 fluorescein in a pH-dependent manner, with NPs formed using more ETOS exhibiting
 121 ‘burst’ release profiles and those formed solely using TEOS displaying ‘slow’ release.

122

123 **Methods**

124 NP synthesis and characterisation: materials, procedures, size and ζ -potential
 125 analysis, TEM studying of NP dissolution are detailed in the Supporting Information

126 FITC-release assay: The degree of FITC release was evaluated by measuring the amount
 127 of dye present in the supernatant and comparing the values measured with the
 128 fluorescent-based calibration curve for FITC at the corresponding pH. The values
 129 achieved from the independent experiments are reported as average ($n = 3$) \pm SD. A

130 Tecan Infinite M200 Pro Safire microplate reader was used for absorbance and
131 fluorescence emission measurements. Samples were added to Nunc Maxisorb 96 well
132 plates before being read (490/525 nm, $\lambda_{ex}/\lambda_{em}$). 250 μg of NP_{TEOS}, NP₅₀₋₅₀ and NP_{ETOS}
133 were washed once by centrifugation and re-dispersion in water before dispersion in 1
134 ml of each phosphate buffer (pH 4, 6 or 7.4). For each sample in each buffer, 7 samples
135 were prepared, one for each timepoint (1, 2, 4, 6, 8, 10, 24hrs) and shaken at 37°C (600
136 rpm). After each incubation time, samples were centrifuged (14000rpm, 10 min) and
137 700 μL of supernatant were removed and the remainder discarded. The pellet isolated
138 after centrifugation was washed twice by centrifugation and re-dispersion in water,
139 then used for TEM analysis.

140 GI tract-like assay: 200 μg of NP_{TEOS}, NP₅₀₋₅₀ and NP_{ETOS} were washed once by
141 centrifugation and re-dispersion in water before dispersion in 1 mL of phosphate
142 buffer at pH 4. The samples were shaken at 37°C (600 rpm). After 2 hours the samples
143 were centrifuged, 300 μL of the supernatant was measured ($\lambda_{ex}/\lambda_{em}$, 490/525 nm,
144 100 μL per well). The remaining NP suspensions were filled with 300 μL of fresh buffer
145 pH 4 and re-incubated. After 2hr the samples were centrifuged and the supernatants
146 completely removed and used for the fluorescence analysis, while the pellets were re-
147 dispersed in 1 mL of buffer at pH 6 and shaken at 37°C (600 rpm). After 2 hours, the
148 samples were centrifuged and the supernatants completely removed and used for the
149 fluorescence analysis, while the pellets were re-dispersed in 1mL of buffer pH 7.4 and
150 shaken again. The samples were centrifuged every 2 hours, 300 μL of the supernatant
151 were used to fill three wells of a 96-well plate and the fluorescence was measured. The
152 experiment was stopped after 12hrs.

153

154 **Results and Discussion**

155 Core-shell microporous SiNPs were synthesised via the reverse microemulsion
156 method^{30,31} and their dissolution in biologically relevant pH was investigated. Different
157 organosiloxane precursors were employed during core formation to produce particles
158 with varying degrees of hydrophobicity and core crosslinking densities. FITC was
159 modified with aminopropyl trimethoxysilane via thiourea bond formation and enabled
160 the dye to be covalently incorporated into the silica matrix during core formation

161 alongside the SiNP precursors (Figure 1).^{31,32} A shell composed of TEOS and negatively
 162 charged phosphonates was then added to each set of particles to insure similar surface
 163 chemistry.³³ From the organosiloxane analogues chosen for this study,
 164 tetraethoxysilane (TEOS), the traditional SiNP precursor, and ethyl triethoxysilane
 165 (ETOS) were the only analogues capable of forming colloids that were stable in
 166 aqueous conditions. These NPs have been named NP_{TEOS} and NP_{ETOS} respectively. TEOS
 167 and ETOS were also added to the microemulsion in equal molar ratios, thus yielding a
 168 third batch of NPs: NP₅₀₋₅₀.

169 Two other siloxanes, bis(triethoxysilyl)benzene and bis(triethoxysilyl)biphenyl,
 170 were also used alongside TEOS as precursors for NP core formation. It was possible to
 171 generate stable NPs in ethanol using both siloxanes but they visually aggregated in less
 172 than one minute when transferred to DI water (Figure S1). Their rapid aggregation was
 173 attributed to the hydrophobic nature of their aromatic moiety and their potential to π -
 174 stack in water, and suggests further surface chemical modification (such as by
 175 PEGylation) would be needed to increase solubility in biological conditions. Even NPs
 176 formed using a 95:5 TEOS:bis(triethoxysilyl)benzene visually aggregated in aqueous
 177 medium (Figure S2).

178
 179 *Table 1: Physicochemical characterisation of the NP_{TEOS}, NP₅₀₋₅₀ and NP_{ETOS} by DLS and TEM. FITC loading per NP*
 180 *was also quantified and allowed for percentage of FITC release to be determined in later dissolution experiments*
 181 *(n=3).*

	DLS			TEM	Loading
	Z-Av. ϕ (nm)	PDI	ζ -potential (mV)	ϕ (nm)	FITC per NP
NP_{TEOS}	132.5 \pm 1.3	0.177 \pm 0.016	-27.8 \pm 0.80	72 \pm 8	1256 \pm 389
NP₅₀₋₅₀	170.0 \pm 2.2	0.147 \pm 0.005	-24.0 \pm 0.27	80 \pm 13	1578 \pm 574
NP_{ETOS}	222.9 \pm 6.0	0.275 \pm 0.030	-22.3 \pm 0.65	50 \pm 31	122 \pm 27

182
 183 The three NPs (NP_{TEOS}, NP₅₀₋₅₀ and NP_{ETOS}) were characterised by DLS and
 184 transmission electron microscopy (TEM) in order to quantify particle size and surface
 185 charge (Table 1). Using TEM, the NP diameters were measured to be 72 \pm 8 nm, 80 \pm 13
 186 nm and 50 \pm 31 nm for NP_{TEOS}, NP₅₀₋₅₀ and NP_{ETOS} respectively. However, using DLS, the
 187 size (Z-average) of the NP_{TEOS}, NP₅₀₋₅₀ and NP_{ETOS} was 132.5 \pm 1.3 nm, 170.0 \pm 2.2 nm,
 188 222.9 \pm 6.0 nm. The NP Z-average size increased with the increasing proportion of ETOS,
 189 which was accompanied by the decrease of the absolute values of overall negative
 190 charge for the three NPs: -27.8 \pm 0.80 mV, -24.0 \pm 0.27 mV, -22.3 \pm 0.65 mV for NP_{TEOS},

191 NP₅₀₋₅₀ and NP_{ETOS}. This inverted correlation suggested that the NPs became less
 192 colloiddally stable and experienced some degree of aggregation when more the
 193 hydrophobic ETOS was used during NP synthesis. No dramatic aggregation over a
 194 period of 2 days was observed for the NP_{TEOS} and NP₅₀₋₅₀ at pH 4, pH 6 and pH 7.4
 195 buffers, but at pH 4, the NP_{ETOS} diameter increased gradually to 1 μ m (Figure 3). This
 196 effect is not desirable for drug delivery systems as increased NP size reduces the overall
 197 surface area-to-volume ratio, which is detrimental to controlled drug release,
 198 significantly changes the size-dependent properties of the NPs and may affect NP-cell
 199 interactions. However, in the case of *in vivo* drug delivery this is unlikely to be
 200 problematic since, in the case of oral administration, the residence time of food in the
 201 stomach is typically 4 hours or less. For intracellular delivery, NPs are likely to be firstly
 202 administered intravenously before reaching a tumour site (i.e. at pH 7.4 where they
 203 are stable). NP localisation in organs usually only then takes a matter of hours, during
 204 which time they are endocytosed and eventually trafficked to late endosomes/
 205 lysosomes (pH 4).

206 The dissolution of SiNPs is well described in the literature and is caused by
 207 hydrolysis of the silica matrix, which is accelerated at higher pH and temperature.^{21,34}
 208 Park et al described the hollowing of SiNPs due to etching under basic conditions.³⁵

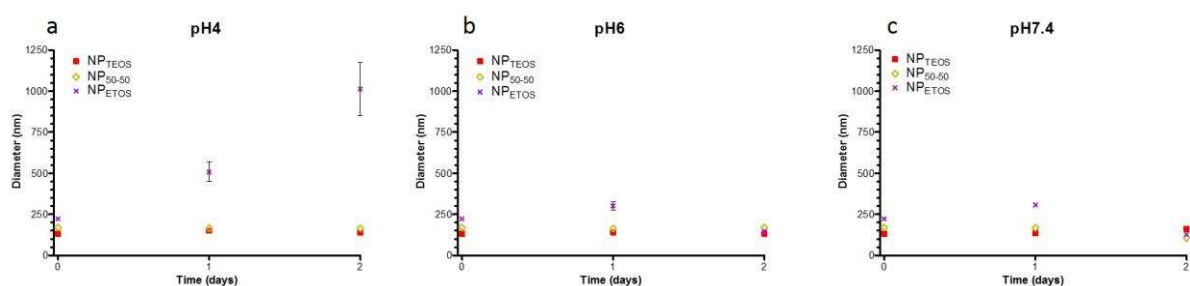


Figure 3: DLS analysis of NP size (Z-average, n=3) over a 2 day period in the pH 4, pH 6 and pH 7.4 buffers. (a) NP_{TEOS} and NP₅₀₋₅₀ were stable over time, but NP_{ETOS} gradually aggregated into micron-sized particles over 48 hours. (b) All NPs remained colloiddally stable for 2 days at pH 6. (c) At pH 7.4, the three sets of NPs also retained their colloiddal stability for 2 days.

209 The authors suggested that small ‘seed pores’ in the particle matrix merge to form
 210 single voids and eventually results in large hollows. Mahon et al. demonstrated that
 211 SiNPs can degrade during *in vitro* cellular experimentation and observed NP hollowing
 212 by TEM following particle incubation in cell culture medium at 37°C.³⁴ We have also
 213 recently observed hollowing in a ‘dissolution assay’ designed to exploit SiNP
 214 degradation as a way to improve immunoassay signal-to-noise ratios.²¹

215 To this end, we have incubated NP_{TEOS}, NP₅₀₋₅₀ and NP_{ETOS} in buffered solutions
 216 at pH 4, pH 6 and pH 7.4 and analysed the NP integrity (i.e. the presence/absence of
 217 cavities/hollows) as an indicator of degradation. Clear changes in NPs morphology
 218 were observed after 6 hours at 37°C (Figure 4), and a complete 24 hour degradation
 219 study by TEM is presented in the Supporting Information (Figure S3, S4, S5). It is
 220 evident from Figure 4 that no changes in particle morphology were found for NP_{TEOS},
 221 NP₅₀₋₅₀ or NP_{ETOS} when incubated at pH4. Small mesopore-sized hollows only became
 222 visible at pH4 in NP_{TEOS} after 24 hours of incubation (Figure S3, S6). This suggests that
 223 the three types of SiNPs would be robust enough to remain intact in the stomach ('fed
 224 state') and presumably also in the 'fasted state' (approx. pH 1.2)^{36,37} because particle
 225 hydrolysis would be slower in more acidic conditions. However, the NPs would not be
 226 capable of intracellular dissolution-based cargo release if the colloids were eventually
 227 trafficked to lysosomes.

228 At pH 6, we noticed that degradation of the colloids had occurred in the NP_{TEOS}
 229 and NP₅₀₋₅₀, but was not evident in the NP_{ETOS} particles. For the NP₅₀₋₅₀ samples, clear
 230 mesopore-scale hollows measuring 13.7±4.9 nm in diameter in the could be seen after

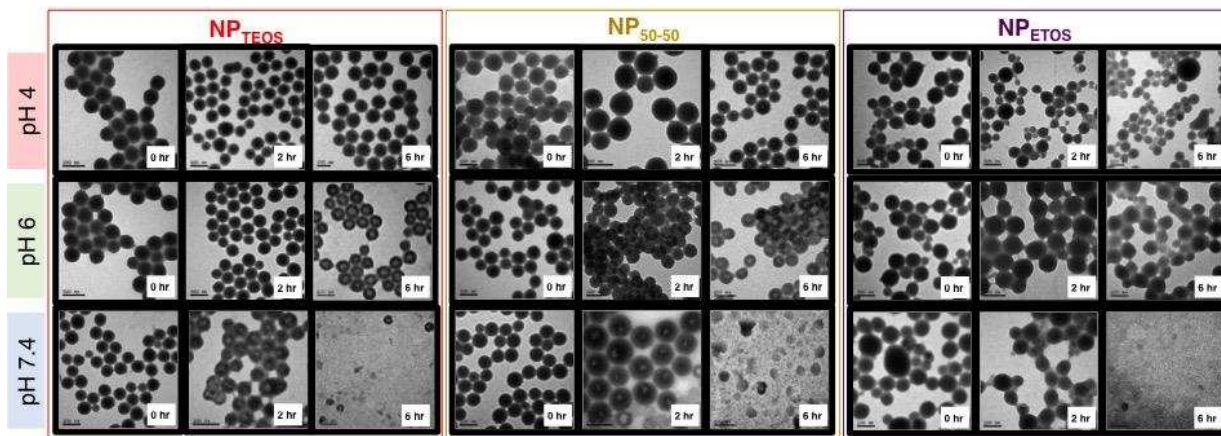


Figure 4: TEM of NP_{TEOS}, NP₅₀₋₅₀, and NP_{ETOS} incubated over time in pH 4, pH 6 and pH 7.4 solutions. No changes in NP morphology were observed in pH 4 over time which suggested silica NPs may be capable of enduring the harsh conditions of the stomach. NPs dissolved in pH 6 and pH 7.4 due to the increased rate of hydrolysis of the silica matrix. Differences were observed in the mode of dissolution of NP_{TEOS} and NP₅₀₋₅₀ compared to NP_{ETOS}: Hollowing of the particle core was present in NP_{TEOS} and NP₅₀₋₅₀, whereas NP_{ETOS} degradation appeared to begin at the particle exterior surface.

231 2 hours and was further evidenced by the micrographs taken from 6 to 24 hours in
 232 which the etching is seen to be further enhanced (Fig S4, S6). NP_{TEOS} did not exhibit
 233 visible degradation at 2 hours at pH 6 but 7.0±3.7 nm hollows were clearly evident
 234 after 6 hours. Such hollowed structures are consistent with those found in other

235 studies focussed on SiNP degradation.^{21,34,35} Interestingly NP_{ETOS} exhibited no visual
236 hollowing in the NP core at pH 6, which is presumably a result of the hydrophobic ethyl
237 groups reducing the presence of water in the silica matrix, thus inhibiting the hydrolysis
238 of the –O-Si-O– bond. Interestingly, it appeared that NP_{ETOS} underwent a dissolution
239 process that led to gradual disintegration of the exterior particle surface. The apparent
240 method of NP_{ETOS} degradation is therefore different to that of NP_{TEOS} and NP₅₀₋₅₀, and
241 is presumably linked to the hydrophobic/hydrophilic nature of the respective particle
242 cores. It is possible that the more hydrophilic cores of NP_{TEOS} and NP₅₀₋₅₀ are susceptible
243 to initial etching by hydrolysis and followed the ‘seed pore’ phenomenon³⁵ to
244 eventually form mesoscopic cavities. On the other hand, the hydrophobic NP_{ETOS} core
245 resisted hydrolysis and dissolution occurred at the particle exterior that was formed
246 only by using TEOS.

247 A striking difference in NP integrity was found for particles incubated in pH 7.4
248 buffer. NP_{TEOS} and NP₅₀₋₅₀ exhibited more severe etching after 2 hours incubation
249 compared to pH 6, which is in agreement with the hypothesis that increased basic
250 conditions lead to more rapid silica hydrolysis and particle dissolution. Indeed, it is
251 clear from the TEM images that NP_{TEOS} and NP₅₀₋₅₀ exhibited an evolution from a
252 microporous structure to a hollowed mesoporous one, which can increase the overall
253 NP surface area and further enhance degradation. This accelerated NP dissolution for
254 both sets of NPs at pH 7.4 caused NP_{TEOS} and NP₅₀₋₅₀ to be largely degraded after 6
255 hours. TEM showed very few intact particles and features observed were
256 predominantly NP debris, which agrees with previous SiNP degradation studies.²¹
257 Further analysis of the NP hollows was conducted by scanning transmission electron
258 microscopy (Figure S7). The results show that the hollowed interior the NPs could
259 eventually etch through to the surface of NP_{TEOS} and NP₅₀₋₅₀ as a way of reducing
260 surface energy,³⁵ and resulted in distinct surface deformations of the NPs.

261 The fact that NP_{TEOS}, NP₅₀₋₅₀ and NP_{ETOS} all degraded at pH7.4 is promising for
262 oral drug delivery as the jejunum (pH 7.4) exhibits larger villi compared to do
263 duodenum (pH 6). This means drugs released at this point in the GI tract would be
264 readily absorbed, thus improving bioavailability before proceeding to enterohepatic
265 circulation. Considering that the NP matrix almost completely disintegrates under
266 these conditions, it may avoid any potential nanotoxicity issues and be cleared from

267 the body. Indeed, silica is used in the food industry as a bulking agent in a number of
268 food products (E551; silicium dioxide) and has been reported to degrade into
269 biocompatible silicic acid.³⁸ However, dissolution of the NPs at pH 7.4 poses a challenge
270 for intracellular delivery as this strategy first involves intravenous NP injection, which
271 exposes the NPs to a pH 7.4 environment, and suggests some of the encapsulated
272 cargo would diffuse from the nanomaterial before localisation. In turn, the total
273 amount of drug transported across the cell membrane would be reduced.

274 Fluorescein isothiocyanate (FITC) was covalently bound inside the core of
275 NP_{TEOS}, NP₅₀₋₅₀ and NP_{ETOS} and served as an indicator of NP degradation. The release
276 profile of FITC into solution can therefore be used to infer the extent of NP dissolution
277 and can be corroborated with the TEM images. Due to the hydrophobic nature of FITC
278 (an analogue for poorly soluble drugs), monitoring the dye release also allowed for
279 concurrent assessment of the release profile of small molecules from the three sets of
280 NPs over time. At each time point, the NPs were centrifuged and intact NPs were
281 concentrated into a pellet, thus allowing the supernatant to be used for analysing free
282 FITC released from the NPs (Figure 2). The quantity of dye released was then
283 extrapolated from the calibration curves of known FITC concentrations prepared at the
284 three different pHs in order to account for FITC's pH-dependent fluorescence emission
285 intensity. The results of this FITC release study are presented in Figure 5.

286 FITC release from NP_{TEOS}, NP₅₀₋₅₀ and NP_{ETOS} was minimal at pH 4 over the course
287 of 24 hours (Figure 5a). The overall concentration of released FITC was less than 5%
288 after 2 hours in the acidic environment and when considering the images of intact NPs
289 obtained via TEM (Figure 4), it suggests that the SiNPs employed in this study would
290 be capable of resisting degradation in the stomach. They may therefore be able to
291 reliably carry drugs to the intestine, and agrees with other reports focussed on silica
292 NP integrity in the stomach and the GI tract as a whole.^{36,37} This was further supported
293 by the fact that less than 10% of FITC was released from NP_{TEOS}, NP₅₀₋₅₀ and NP_{ETOS} at
294 pH 4 after 24 hours. In addition, the low release rate of the dye into solution suggested
295 SiNPs intracellularly trafficked to late endosomes/lysosomes would not release
296 encapsulated cargo via NP dissolution and alternative strategies of ensuring drug
297 delivery would be needed. For example, strategies like changes to NP shape or surface
298 chemistry may ensure escape from intracellular vesicles into the more dissolution-

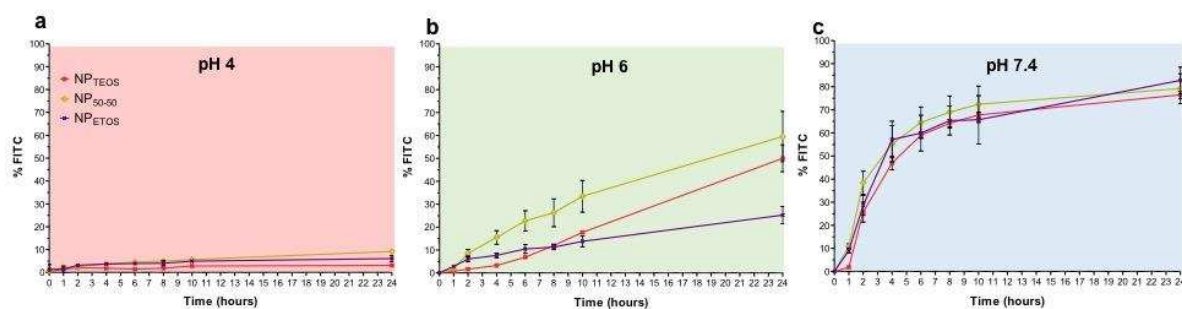


Figure 5: FITC release from the NPs over time when incubated in gastrointestinal pH's. (a) NPs were incubated in pH 4 solution and little FITC was detected in the sample supernatant over a 24 hour period. (b) In pH 6 gradual FITC release was observed and was attributed to increased hydrolysis rate compared to pH 4. (c) NP degradation was most rapid in pH 7.4 and release the majority of the FITC cargo into solution over time.

299 friendly conditions of the cytosol (pH 7 - 7.4),³⁹⁻⁴¹ thus avoiding potential NP
 300 exocytosis.⁴²

301 At pH 6, an increase in dye release was seen over time for the three NP
 302 formulations, although NP_{TEOS} releases FITC at a slower rate than both NP₅₀₋₅₀ and
 303 NP_{ETOS} in the first 8 hours (Figure 5b). This is likely due to the more highly crosslinked
 304 nature of the core formed solely from TEOS, which results in slower dye diffusion out
 305 of NP_{TEOS}. Nonetheless, it is clear that increasing the pH from 4 to 6 led to more rapid
 306 dye release from the NPs and is attributed to the increased rate of hydrolysis at higher
 307 pH causing particle dissolution.

308 The fluorescence data of the NPs at pH 7.4 clearly showed that dye release due
 309 to NP degradation allowed for more rapid release of FITC (Figure 5c). This result
 310 correlated well with the electron microscopy results (Figure 2, S3, S4, S5 S6) from which
 311 it is evident that extensive particle dissolution occurred after 6 hours. More than 55%
 312 of FITC was released from NP_{TEOS}, NP₅₀₋₅₀ and NP_{ETOS} after 6 hours, which, in the case of
 313 oral drug delivery, suggested that small intestine would be the location where the
 314 majority of drugs would become available for absorption. This is clearly positive as this
 315 would lead to more efficacious delivery of the therapeutic. The loss of dye at pH 7.4
 316 may not be beneficial for intracellular delivery as the cargo can be released before
 317 localising at tumour sites and prior to endocytosis. The fluorescence data also agrees
 318 with the findings of Mahon *et al.* where dye-leaching from SiNPs caused by NP
 319 dissolution can occur at physiological pH *in vitro*.³⁴ The authors then developed an
 320 alternative SiNP synthetic approach to prevent SiNP dissolution and dye-leaching in *in*
 321 *vitro* conditions.

322 Considering the favourable fluorescein retention in acidic conditions and
 323 release at higher pH, we decided to investigate whether the microporous SiNPs
 324 synthesised in this study may be suited to oral drug delivery. FITC release was
 325 monitored over time while increasing the pH, in an attempt to mimic the pH conditions
 326 of the whole GI tract and the digestion process (i.e. stomach, pH 4, to duodenum, pH6,
 327 to jejunum, pH 7.4, Figure 6a). The results are summarised in Figure 6b as free data
 328 points.

329 As expected, at pH 4 the NPs released less than 10% of the FITC cargo over a 4-hour
 330 period. However, when the pH increased to 6 a difference in dye release was observed
 331 for NP_{TEOS}, NP₅₀₋₅₀ and NP_{ETOS}. NP₅₀₋₅₀ release was higher than NP_{TEOS} and NP_{ETOS} at pH
 332 6 solution. However, the most dramatic trend was the 'burst release' profile of FITC
 333 from NP_{ETOS} whilst incubated at pH 6 and pH 7.4. Only 3% of the FITC cargo was
 334 released at pH 4 over 4 hours, but once the NP_{ETOS} experienced small intestine-like
 335 conditions, the rate of release rapidly increased and 70% of dye was released into
 336 solution after 8 hours. The overall release of FITC from NP_{ETOS} was 80% after 12 hours.
 337 While NP₅₀₋₅₀ showed the highest release of FITC at pH 6, no dramatic increase in
 338 release was observed at pH 7.4, with 62% of the loaded FITC was detected in the

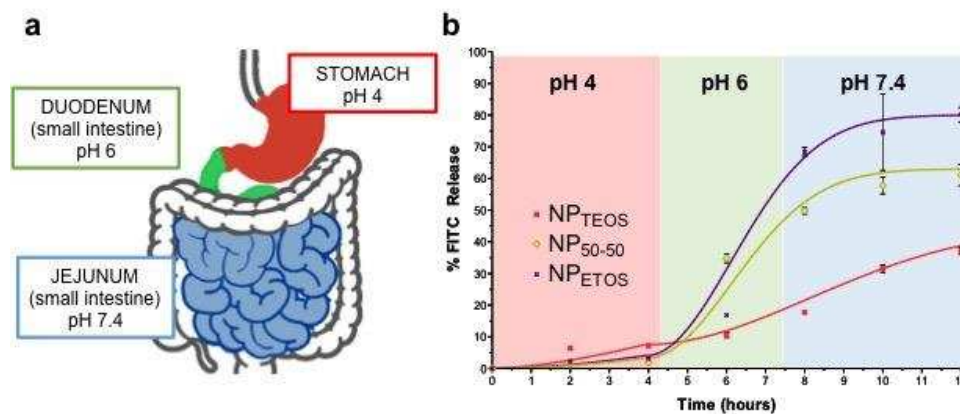


Figure 6: (a) The pathway through the gastrointestinal tract was mimicked over time. Stomach pH (pH 4) refers to that of 'fed state' and the requirement for some therapeutics like nonsteroidal anti-inflammatory drugs to be administered concurrently with food ingestion (b) Marginal FITC was released at pH4. Then, a pH-dependent dye release profile was observed for the respective NPs. NP_{TEOS} released FITC slowly and in a sustained manner at pH 6 and pH 7.4. NP₅₀₋₅₀ and NP_{ETOS} displayed initial burst release at pH 6 followed by a steady release at pH 7.4. Greater dye retention in the NPs was observed when increased TEOS was used for core formation. The free data points were used to manually fit Higuchi-Peppas models.

339 supernatant after 12 hours. On the other hand, NP_{TEOS} exhibited slow dye release at pH
 340 6 and pH 7.4 and released less than 40% of its fluorescent cargo after 12 hours.

341 To further understand the FITC release from the NP_{TEOS}, NP₅₀₋₅₀ and NP_{ETOS}
 342 presented in Figure 6b, the Peppas kinetic model was considered as an appropriate

343 model to assess diffusion-based cargo release from drug delivery systems.^{43,44} The
344 model is typically applied to polymeric systems (SI, Equations 1 and 2). The dye release
345 was simulated for NP_{TEOS}, NP₅₀₋₅₀ and NP_{ETOS} and the simulated profiles appeared to fit
346 the experimental observations well. The same rate constants were used for the fitting
347 of the NP₅₀₋₅₀ and NP_{ETOS} data which suggests the incorporation of ETOS in the NP core
348 led to similar dye diffusion pathways for the two types of colloid. However, the higher
349 retention of FITC by NP₅₀₋₅₀ compared to NP_{ETOS} suggested that the former presumably
350 had a more densely formed silica matrix that eventually limited the release of the dye
351 during the time period studied. Different rate constants were needed to fit the NP_{TEOS}
352 data and suggested a different overall FITC release mechanism compared to both NP₅₀₋₅₀
353 and NP_{ETOS}. This is consistent with the hypothesis where a higher crosslinking density
354 in a NP core matrix formed from TEOS alone and was reflected by the higher retention
355 of FITC after 12 hours. The results presented in Figure 6b therefore show that
356 increasing the amount of ETOS during NP synthesis would lead to increased cargo
357 release at the pH found in small intestine (i.e. pH 6 and 7.4). This may prove beneficial
358 if a 'burst release' profile is desirable, whereas it would be preferable to employ NPs
359 formulated solely from TEOS for slower molecular release into the small intestine.

360 These findings established that SiNPs exhibit pH-dependent dissolution profiles,
361 and it is possible to synthesise SiNPs that exhibit different cargo release profiles that
362 hold potential in oral drug delivery applications. The ease at which these microporous
363 NPs were synthesised and shown to exhibit different dissolution behaviour suggests
364 that a number of further studies should be performed with encapsulated molecules of
365 various physicochemical properties. We have also previously developed
366 methodologies for extending SiNP storage and long-term stability,^{22,45} and implied that
367 the successful approaches for synthesising microporous SiNP with drug molecules
368 could potentially be developed into realistic nano-delivery systems. In addition, the
369 particles presented here may also be applicable to the emerging field of nano-
370 nutraceuticals;^{1,44,46} a field concerned with tuning molecule release kinetics and
371 absorption using nano-sized carriers for more effective nutrient delivery systems. The
372 use of microporous SiNPs therefore offers a number of potential routes for improved
373 transport, protection and release of therapies in oral drug delivery and indeed the drug
374 delivery field as a whole.

375

376 **Conclusion**

377 Microporous SiNPs with core-shell architecture were synthesised and their dissolution
378 in biologically relevant pH (pH 4, pH 6, pH 7.4) was assessed. These pH refer to those
379 found intracellularly and in the gastrointestinal tract. NP cores were formed using
380 tetraethoxysilane (NP_{TEOS}), ethyl triethoxysilane (NP_{ETOS}) or a 1:1 ratio of both
381 precursors (NP₅₀₋₅₀). These NPs did not degrade in pH 4 conditions but exhibited
382 degradation and fluorescein-release at pH 6 and pH 7.4. This was attributed to
383 accelerated hydrolysis of the silica matrix at higher pH, the formation of mesopore-
384 sized hollows and subsequent NP dissolution. This suggested that dissolution-based
385 cargo release from the NPs presented here may be more likely to diffuse from of the
386 NPs at physiological pH (pH 7.4) before being endocytosed and entering intracellular
387 vesicles (pH 6 – early endosome, pH 4 - late endosome/lysosome). The degradation of
388 the NPs at pH 7.4 also infers that this class of nanomaterial could be safely cleared and
389 excreted. On the other hand, the retention of the fluorescein cargo in acidic conditions
390 meant the NPs could be applicable to oral drug delivery where drugs required
391 protection in the stomach. In a mimicked gastrointestinal tract study, increasing the
392 amount of ETOS in the NP core formation led to increased release of FITC in pH 6 and
393 pH 7.4 solutions. The release profiles of FITC are consistent with the hypothesis that
394 cargo release from the NPs is controlled in part by the crosslinking density of the silica
395 core, with ETOS generating a less dense matrix that facilitates greater cargo release at
396 small intestinal pH (pH 6 and pH 7.4). The data obtained for NP_{TEOS} suggests this class
397 of SiNP would be more suited to slow drug release in oral drug delivery applications.
398 Overall, while further studies are needed to elucidate the degradation mechanisms
399 associated with the colloidal systems presented here, we showed that it was possible
400 to tune the release of encapsulated from SiNPs by simply changing the precursor used
401 during NP synthesis. Microporous SiNPs therefore hold potential as a flexible platform
402 upon which to base oral drug delivery strategies.

403

404 **Acknowledgements:** GG thanks the University of Kent for the provision of her PhD
405 scholarship

406 **References**

- 407 1 J. Gleeson, S. Ryan and D. Brayden, *Trends in Food Science & Technology*, 2016, **53**, 90-101
408 (DOI:10.1016/j.tifs.2016.05.007).
- 409 2 A. Tivnan, W. Orr, V. Gubala, R. Nooney, D. Williams, C. McDonagh, S. Prenter, H. Harvey,
410 R. Domingo-Fernandez, I. Bray, O. Piskareva, C. Ng, H. Lode, A. Davidoff and R. Stallings,
411 *PLoS One*, 2012, **7**, e38129 (DOI:10.1371/journal.pone.0038129).
- 412 3 L. Chuah, C. Roberts, N. Billa, S. Abdullah and R. Rosli, *Coll. Surf B Biointerfaces*, 2014, **116**,
413 228-236 (DOI:10.1016/j.colsurfb.2014.01.007).
- 414 4 H. Amekyeh, N. Billa and C. Roberts, *Int. J. Pharm.*, **517**, 42-49
415 (DOI:10.1016/j.ijpharm.2016.12.001).
- 416 5 C. Lien, É Molnař, P. Toman, J. Tsibouklis, G. Pilkington, D. Gořeckı and E. Barbu,
417 *Biomacromolecules*, 2012, **13**, 1067-1073 (DOI:10.1021/bm201790s).
- 418 6 C. Saraiva, C. Praça, R. Ferreira, T. Santos, L. Ferreira and L. Bernardino, *J. Contr. Rel.*, 2016,
419 **235**, 34-47 (DOI:10.1016/j.jconrel.2016.05.044).
- 420 7 F. Barandeh, P. Nguyen, R. Kumar, G. Iacobucci, M. Kuznicki, A. Kosterman, E. Bergey, P.
421 Prasad and S. Gunawardena, *PLoS One*, 2012, **7**, e29424
422 (DOI:10.1371/journal.pone.0029424).
- 423 8 J. Florek, R. Caillard and F. Kleitz, *Nanoscale*, 2017, **9**, 15252-15277
424 (DOI:10.1039/C7NR05762H).
- 425 9 E. Phillips, O. Penate-Medina, P. Zanzonico, R. Carvajal, P. Mohan, Y. Ye, J. Humm, M.
426 Gönen, S. Kalaigian H., H. Strauss, S. Larson, U. Wiesner and M. Bradbury, *Sci. Trans. Med*,
427 2014, **6**, 260ra149 (DOI:10.1126/scitranslmed.3009524).
- 428 10 Y. Yang, Z. Song, B. Cheng, K. Xiang, X. Chen, J. Liu, A. Cao, Y. Wang, Y. Liu and H. Wang, *J.*
429 *Applied Toxicology*, 2013, **34**, 424-435 (DOI:10.1002/jat.2962).
- 430 11 R. Guillet-Nicolas, A. Popat, J. Bridot, G. Monteith, S. Qiao and F. Kleitz, *Angew. Chem.*
431 *Int. Ed.*, 2013, **52**, 2318-2322 (DOI:10.1002/anie.201208840).
- 432 12 L. Li, T. Liu, C. Fu, L. Tan, X. Meng and H. Liu, *Nanomedicine: Nanotechnology, Biology and*
433 *Medicine*, 2015, **11**, 1915-1924 (DOI:10.1016/j.nano.2015.07.004).
- 434 13 A. Popat, S. Jambhrunkar, J. Zhang, J. Yang, H. Zhang, A. Meka and C. Yu, *Chem. Comm.*,
435 2014, **50**, 5547-5550 (DOI:10.1039/C4CC00620H).
- 436 14 Z. Li, J. Barnes, A. Bosoy, J. Stoddart and J. Zink, *Chem. Soc. Rev.*, 2012, **41**, 2590-2605
437 (DOI:10.1039/C1CS15246G).

- 438 15 L. McCusker, F. Liebau and G. Engelhardt, *Pure Appl. Chem.*, 2001, **73**, 381-394.
- 439 16 M. Thommes, K. Kaneko, A. Neimark, J. Olivier, F. Rodriguez-Reinoso, J. Rouquerol and K.
440 Sing, *Pure Appl. Chem.*, 2015, **87**, 1051-1069 (DOI:10.1515/pac-2014-1117).
- 441 17 T. Ohulchanskyy, I. Roy, L. Goswami, Y. Chen, E. Bergey, R. Pandey, A. Oseroff and P.
442 Prasad, *Nano Lett.*, 2007, **7**, 2835-2842 (DOI:10.1021/nl0714637).
- 443 18 B. Riva, M. Bellini, E. Corvi, P. Verderio, E. Rozek, B. Colzani, S. Avvakumova, A.
444 Radeghieri, M. Rizzuto, C. Morasso, M. Colombo and D. Prospero, *J. Coll. Interface Sci.*, 2018,
445 **519**, 18-26 (DOI:10.1016/j.jcis.2018.02.040).
- 446 19 L. Tang and J. Cheng, *Nanotoday*, 2013, **8**, 290-312 (DOI:10.1016/j.nantod.2013.04.007).
- 447 20 R. Nooney, A. White, C. O'Mahony, C. O'Connell, K. Kelleher, S. Daniels and C. McDonagh,
448 *J. Coll. Interface Sci.*, 2015, **456**, 50-58 (DOI:10.1016/j.jcis.2015.05.051).
- 449 21 C. Moore, G. Giovannini, F. Kunc, A. Hall and V. Gubala, *J. Mater. Chem. B*, 2017, **5**, 5564-
450 5572 (DOI:10.1039/C7TB01284E).
- 451 22 C. Moore, H. Montón, R. O'Kennedy, D. Williams, C. Nogués, C. Crean (neé Lynam) and V.
452 Gubala, *J. Mater Chem. B*, 2015, **3**, 2043-2055 (DOI:10.1039/C4TB01915F).
- 453 23 M. Benezra, O. Penate-Medina, P. Zanzonico, D. Schaer, H. Ow, A. Burns, E. DeStanchina,
454 V. Longo, E. Herz, S. Iyer, J. Wolchok, S. Larson, U. Wiesner and M. Bradbury, *J. Clin. Invest.*,
455 2011, **121**, 2768-2780 (DOI:10.1172/JCI45600).
- 456 24 J. Fuller, G. Zugates, L. Ferreira, H. Ow, N. Nguyen, U. Wiesner and R. Langer,
457 *Biomaterials*, 2012, **29**, 1526-1532 (DOI:10.1016/j.biomaterials.2007.11.025).
- 458 25 M. Ruedas-Rama, J. Walters, A. Orte and E. Hall, *Analytica Chimica Acta*, 2012, **751**, 1-23
459 (DOI:10.1016/j.aca.2012.09.025).
- 460 26 F. Aureli, M. D'Amato, B. De Berardis, A. Raggi, A. Turcoa and F. Cubadda, *J. Anal. At.*
461 *Spectrom.*, 2012, **27**, 1540-1548 (DOI:10.1039/C2JA30133D).
- 462 27 E. Choi and S. Kim, *Langmuir*, 2017, **20**, 4974-4980 (DOI:10.1021/acs.langmuir.7b00332).
- 463 28 N. Summerlin, Z. Qua, N. Pujara, Y. Sheng, S. Jambhrunkar, M. McGuckin and A. Papat,
464 *Coll. Surf. B*, 2016, **144**, 1-7 (DOI:10.1016/j.colsurfb.2016.03.076).
- 465 29 H. Yamada, C. Urata, Y. Aoyama, S. Osada, Y. Yamauchi and K. Kuroda, *Chem. Mater.*,
466 2012, **24**, 1462-1471 (DOI:10.1021/cm3001688).
- 467 30 R. Bagwe, C. Yang, L. Hilliard and W. Tan, *Langmuir*, 2004, **20**, 8336-8342
468 (DOI:10.1021/la049137j).

469 31 R. Nooney, E. McCormack and C. McDonagh, *Anal. Bioanal. Chem.*, 2012, **404**, 2807-2818
470 (DOI:doi: 10.1007/s00216-012-6224-z).

471 32 A. Van Blaaderen and A. Vrij, *Langmuir*, 1992, **8**, 2921-2931 (DOI:10.1021/la00048a013).

472 33 R. Bagwe, L. Hilliard and W. Tan, *Langmuir*, 2006, **22**, 4357-4362
473 (DOI:10.1021/la052797j).

474 34 E. Mahon, D. Hristov and K. Dawson, *Chem. Commun.*, 2012, **48**, 7970-7972
475 (DOI:10.1039/C2CC34023B).

476 35 S. Park, Y. Kim and S. Park, *Langmuir*, 2008, **24**, 12134-12137 (DOI:10.1021/la8028885).

477 36 C. Frujtier-Pölloth, *Archives of Toxicology*, 2016, **90**, 2885-2916 (DOI:10.1007/s00204-
478 016-1850-4).

479 37 H. Winkler, M. Suter and H. Naegel, *Journal of Nanobiotechnology*, 2016, **14**, 44
480 (DOI:10.1186/s12951-016-0189-6).

481 38 J. Park, L. Gu, G. von Maltzahn, E. Ruoslahti, S. Bhatia and M. Sailor, *Nat. Mater.*, 2009, **8**,
482 331-336 (DOI:10.1038/nmat2398).

483 39 Z. Chu, S. Zhang, B. Zhang, C. Zhang, C. Fang, I. Rehor, P. Cigler, H. Chang, G. Lin, R. Liu
484 and Q. Li, *Scientific Reports*, 2014, **4**, 4495 (DOI:10.1038/srep04495).

485 40 Z. Chu, K. Miu, P. Lung, S. Zhang, S. Zhao, H. Chang, G. Lin and Q. Li, *Scientific Reports*,
486 2015, **5**, 11661 (DOI:10.1038/srep11661).

487 41 E. Lukianova-Hleb, A. Belyanin, S. Kashinath, X. Wu and D. Lapotko, *Biomaterials*, 2012,
488 **33**, 1821-1826 (DOI:10.1016/j.biomaterials.2011.11.015).

489 42 R. Yanes, D. Tarn, A. Hwang, D. Ferris, S. Sherman, C. Thomas, J. Lu, A. Pyle, J. Zink and F.
490 Tamanoi, *Small*, 2013, **9**, 697-704 (DOI:10.1002/sml.201201811).

491 43 J. Siepmann and N. Peppas, *Int. J. Pharm.*, 2011, **418**, 6-12 (DOI:10.1016/j.ijpharm.
492 2011.03.051).

493 44 M. Danish, G. Voza, H. Byrne, J. Frias and S. Ryan, *Innovative Food Science and Emerging
494 Technologies*, 2017, (DOI:10.1016/j.ifset.2017.07.002).

495 45 G. Giovannini, F. Kunc, C. Piras, O. Stranik, A. Edwards, A. Hall and V. Gubala, *RSC Adv.*,
496 2017, **7**, 19924-19933 (DOI:10.1039/C7RA02427D).

497 46 M. Danish, G. Voza, H. Byrne, J. Frias and S. Ryan, *J. Food Science*, 2017,
498 (DOI:10.1111/1750-3841.13824).

499

500

501

502

503

504

505

506

507

508

509

510

511

512

513

514

515

516

517

518

Supporting Information

519

520

pH-Dependent Silica Nanoparticle Dissolution and Cargo Release

521

522 Giorgia Giovaninnij,^a Colin J. Moore,^b ^{‡*} Andrew J. Hall,^a Hugh J. Byrne,^b Vladimir Gubala^a

523

524 ^aMedway School of Pharmacy, University of Kent, Central Ave, Chatham Maritime, Kent,
525 ME4 4TB, United Kingdom

526 ^bFOCAS Research Institute, Dublin Institute of Technology, Kevin St., Dublin 8, Ireland

527

528 Email: gg238@kent.ac.uk, colin.moore@dit.ie, a.hall@kent.ac.uk, hugh.byrne@dit.ie,
529 v.gubala@kent.ac.uk

530

531 *Corresponding author: colin.moore@dit.ie , Tel: +353 1 4027902 , Fax: +353 1 4027901

532

533

534 [‡]Current address: EA 6295 Nanomedicine and Nanoprobes, Faculty of Pharmacy, University
535 of Tours, 31 venue Monge, Tours, 37200, France

536

537

538

539

540

541

542

543

544

545 **Additional experimental information**

546 Materials

547 Cyclohexane (anhydrous, 99.5%), 1-hexanol (anhydrous, 99%), Triton[®] X-100,
548 aminopropyl trimethoxysilane [APTMS] (97%), tetraethoxysilane[TEOS] (99.99%),
549 ethyltriethoxysilane (96%)[ETOS], 4,4'-Bis(triethoxysilyl)biphenyl (95%) [bis(TE)PP], 4,4'-

550 Bis(triethoxysilyl)benzene (96%) [bis(TE)B], ammonium hydroxide solution (28% w/v in
551 water, $\geq 99.99\%$), 3-(trihydroxysilyl)propyl methylphosphonate monosodium salt (42%
552 w/v in water) [THPMP], fluorescein isothiocyanate isomer I ($\geq 90\%$)[FITC], sodium
553 phosphate dibasic ($>98.5\%$), sodium phosphate monobasic ($>98\%$), sodium carbonate
554 ($\geq 99.5\%$), sodium bicarbonate ($\geq 99.5\%$), were purchased from Sigma Aldrich. Sodium
555 carbonate (0.1M) combined with sodium bicarbonate (0.1M) yielded pH10.6 (9:1 v/v
556 respectively) solutions. Absolute ethanol, transparent Nunc Maxisorb 96 well plates
557 were purchased from Fisher Scientific. Carbon Films on 400 Mesh Grids Copper were
558 purchased from Agar Scientific.

559 Nanoparticle synthesis

560 Dye precursor formation: In a dried glass vial, FITC (2.5 mg) was dissolved in 1-hexanol
561 (2mL) with APTMS (5.6 μL). The reaction was stirred for 2 hours under a nitrogen
562 atmosphere.

563 All nanoparticles were formed in a microemulsion prepared by combining
564 cyclohexane (7.5 mL), 1-hexanol (1.133 mL), Triton[®] X-100 (1.894 g) and DI water
565 (0.48 mL) in a 30 mL plastic bottle under constant stirring. For the formation of the
566 silica core, TEOS and ETOS were added in different ratios with quantity of oxysilane
567 being equal 0,45 mmol.

568

569

570

571

	TEOS % (μL)	ETOS % (μL)
--	--------------------------	--------------------------

NP _{TEOS}	100% (100)	/
NP ₅₀₋₅₀	50% (50)	50% (48)
NP _{ETOS}	/	100% (97)

572

573 Dye precursor solution (0.162 mL) was then added. After 30 minutes, 40 μ L of
574 ammonium hydroxide was added to trigger polymerisation. The mixture was stirred
575 for further 24 hours. Nanoparticle shells were synthesised by adding 50 μ L of TEOS. 20
576 minutes later 40 μ L THPMP was added. After 5 minutes, 10 μ L of APTMS was then
577 added, and the mixture was allowed to stir at RT for another 24hrs. The microemulsion
578 was then broken by adding 30 mL ethanol. Formed SiNPs were purified by
579 centrifugation (14000 rpm, 10 min) and re-dispersion in ethanol (x3). After purification,
580 the NPs were stored in ethanol at 4°C.

581 Quantification of FITC loading

582 In order to quantify the amount of FITC loaded during the synthetic procedure, 200 μ g
583 of each type of SiNPs were shaken (600 rpm) at 37°C in sodium carbonate/sodium
584 bicarbonate (1:9) buffer at pH10.6 as previously reported.²¹ After 5 hours, the samples
585 were centrifuged (14000 rpm, 10 min) and no pellet was observed, meaning that the
586 particles had dissolved. Three wells of the 96-well plate were filled with 200 μ L of the
587 supernatant isolated after centrifugation. The signal given by FITC molecules free in
588 solution was compared to a fluorescence/absorbance-based calibration curve of
589 known concentrations of FITC at pH10.6. The amount of dye loaded in 200 μ g of
590 particle were calculated. From the values obtained, the number of molecules per NP
591 was calculated by using the spherical volume of the silica NPs calculated from average
592 TEM diameters. The signal was read at 490/525 nm ($\lambda_{ex}/\lambda_{em}$). Values are reported as
593 average of three independent batches of particles (n=3) \pm SD.

594

595

596 Synthesis of NPs using benzene-oxysilanes

597 The same microemulsion and FITC-loading setup as described above was used except
 598 for the choice of oxysilanes. Again, a total of 0.45mmol of oxysilane was used. TEOS
 599 was used for NP formation alongside either bis(triethoxysilyl)benzene [bis(TE)B] or
 600 bis(triethoxysilyl)biphenyl [bis(TE)PP].

TEOS:Bis(TE) B	TEOS [μL]	Bis(TE)B [μL]
95:5	95	8.92
90:10	90	17.85
85:15	85	26.77
75:25	75	44.62
50:50	50	89.24
TEOS:Bis(TE) PP	TEOS [μL]	Bis(TE)PP [μL]
75:25	75	51.44
50:50	50	102.88

601

602 Nanoparticle shells were synthesised by adding 50 μL of TEOS, followed by 40 μL of
 603 THPMP and 10 μL of APTMS after 20min and 5min between each other. After 24h, the
 604 microemulsion was broken by adding 30 mL ethanol. Formed SiNPs were purified by
 605 centrifugation (14000 rpm, 10 min) and re-dispersion in ethanol (3x). After purification,
 606 the nanoparticles were stored in ethanol at 4°C.

607 Buffer preparation

608 Phosphate buffer at different pH were prepared mixing 0.2 M sodium phosphate
609 dibasic and 0.2 M sodium phosphate monobasic and adjusting the pH to 4, 6 and 7.4
610 using 5 M NaOH and 5 M of HCl.

611

612 NP characterization

613 *Dynamic light scattering and zetametry:* SiNPs were dispersed at a concentration of
614 500µg/mL in DI water. Their size and zeta-potential were analysed in a disposable
615 folded capillary cell (DTS1070) at RT using Malvern Zetasizer. n = 3, average ± SD.

616 *SiNP stability:* 250µg/mL of NP_{TEOS}, NP₅₀₋₅₀ and NP_{ETOS} were isolated and re-dispersed
617 in 1mL of each buffer (pH 4, 6 and 7.4) and incubated at 37°C. Size and zeta potential
618 were measured by DLS at 0hr, 24hr, 48hr using Malvern Zetasizer. n = 3, average ± SD.

619 *Transmission electron microscopy:* NP size quantification following synthesis: 5µL of
620 NPs in water (500µg/mL) was added on 'Carbon Films on 400 Mesh Grids Copper'
621 (Agar Scientific) and allowed to evaporate. Using ImageJ software, at least 100 NPs
622 per image were analysed for NP diameter.

623 *SiNPs dissolution using TEM:* Following incubation in pH 4, 6, or 7.4 over different
624 times, NP pellets were isolated using centrifugation (x3), washed using DI water in
625 order to remove residues salts. The pellet was finally re-dispersed in 200µL DI water,
626 3µL added to 'Carbon Films on 400 Mesh Grids Copper' (Agar Scientific) and allowed
627 to evaporate. Images were taken on a Joel JEM-3200FS at ×250, ×200, ×150 and ×100
628 magnification.

629

630 *Scanning Transmission Electron Microscopy (STEM): SiNPs dissolution:* The same grids
631 as 'SiNPs dissolution using TEM' prepared for TEM analysis for the main text were used
632 for STEM. The grids were analysed in STEM imaging mode using a Hitachi SU-6600
633 microscope. Images were taken in secondary electron (SE) and transmission electron
634 (TE) mode at 130,000 magnification using either 20kV or 25kV accelerating voltage.
635 The working distance was 8mm.

636

637 Data fitting of with Peppas model for data points in Figure 6b

638 The data from the release profile of the 'GI tract-like assay' was manually simulated
 639 with SigmaPlot using the diffusive models presented by Siepmann and Peppas.⁴³
 640 Equation 1 was used to fit data from 0 to 4 hours.

641
$$\frac{M_t}{M_\infty} = (k_{s1})(\sqrt{time}) + (k_{s2})(time)$$

642 [Eq. 1]

643 where M_t is the diffused mass at a given time, M_∞ is the asymptotic diffused mass at
 644 infinite time, k_{s1} and k_{s2} are diffusive and relaxation constants. Equation 2 was used to
 645 fit the data from 4 to 12 hours.

646
$$\frac{M_t}{M_\infty} - \frac{M_4}{M_\infty} = (k_{i1})(\sqrt{time - 4}) + (k_{i2})(time - 4)$$

647 [Eq. 2]

648 where M_4 is the predicted diffused mass at the time of changing from pH4 to pH6 (i.e.
 649 after 4 hours). The rate constants used to for Equation 1 and 2 are presented below.
 650 M_∞ for NP_{TEOS}, NP₅₀₋₅₀ and NP_{ETOS} were 45, 63 and 80 respectively.

	NP _{TEOS}	NP ₅₀₋₅₀	NP _{ETOS}
k_{s1}	0.02	0.0025	0.0025
k_{s2}	0.01	0.005	0.005
k_{i1}	0.01	0.001	0.001
k_{i2}	0.05	0.2	0.2

651

652

653

654 **Supporting Figures**

655

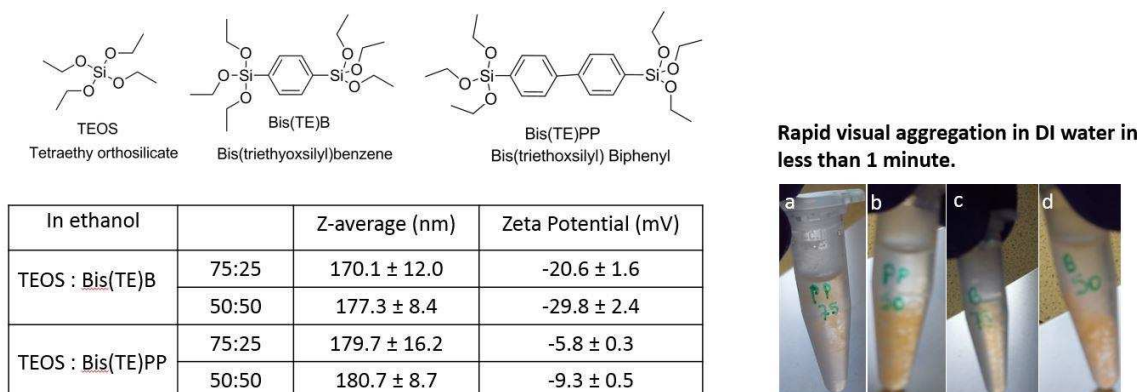


Figure S1: FITC-doped silica NPs were formed by combining the traditional precursor TEOS and either bis(triethoxysilyl)benzene, Bis(TE)B, or bis(triethoxysilyl)biphenyl, Bis(TE)PP. The ratio TEOS:Bis(TE)B and TEOS:Bis(TE)PP was 75:25 and 50:50. The resultant colloids were soluble in ethanol and dynamic light scattering was used to quantify the diameter and zeta potential of the NPs (n=3), as shown in the above table. However, when they were dispersed in DI water the NPs visually aggregated in less than 1 minute. [a , b : TEOS:Bis(TE)B 75:25, 50:50]; c, d: TEOS:Bis(TE)PP]

656

657

658

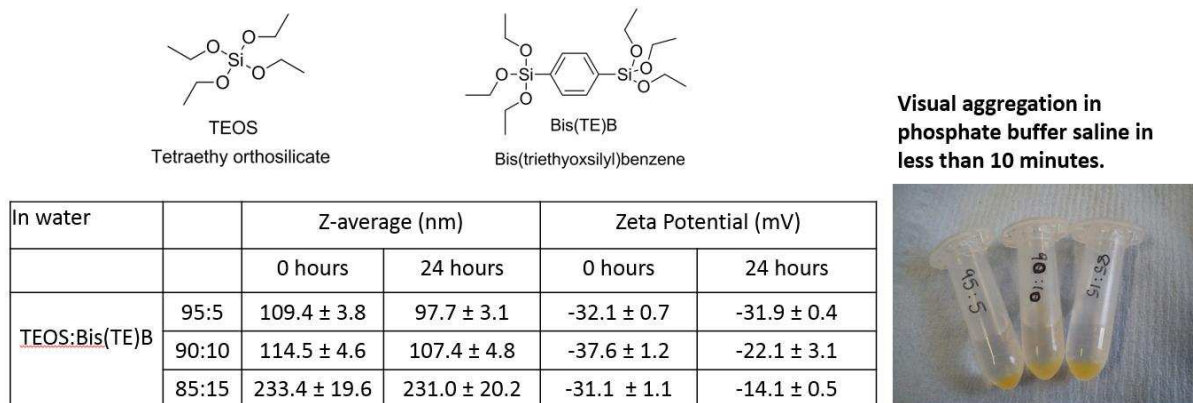


Figure S2: Bis(TE)B was incorporated in to FITC-loaded silica NPs in lower molar concentrations as a way make the resultant NPs 'less hydrophobic' and therefore stable in aqueous conditions. TEOS:Bis(TE)B was added to the microemulsion in 95:5, 90:10, 85:15 and were colloidal stable in DI water for 24 hours. However when the NPs were dispersed in PBS they visually aggregated after only 10 minutes.

pH4

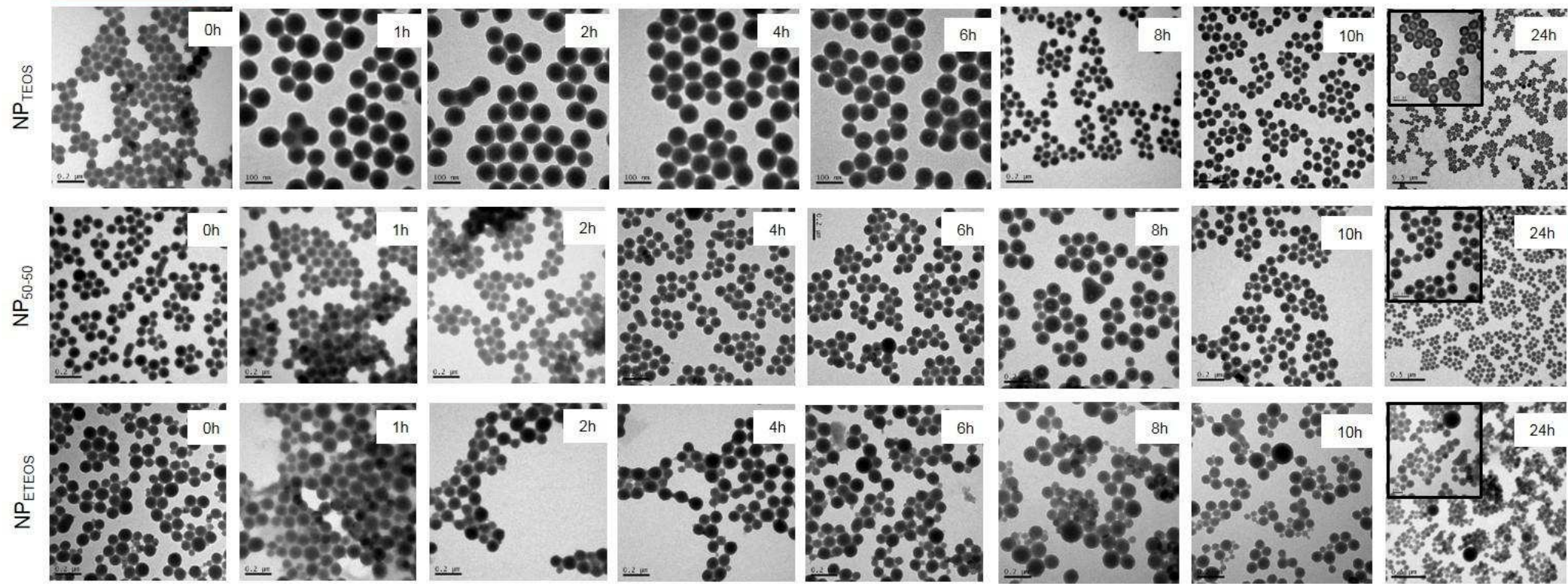


Figure S3: The three sets of NPs appeared in tact when incubated over time in pH 4

pH 6

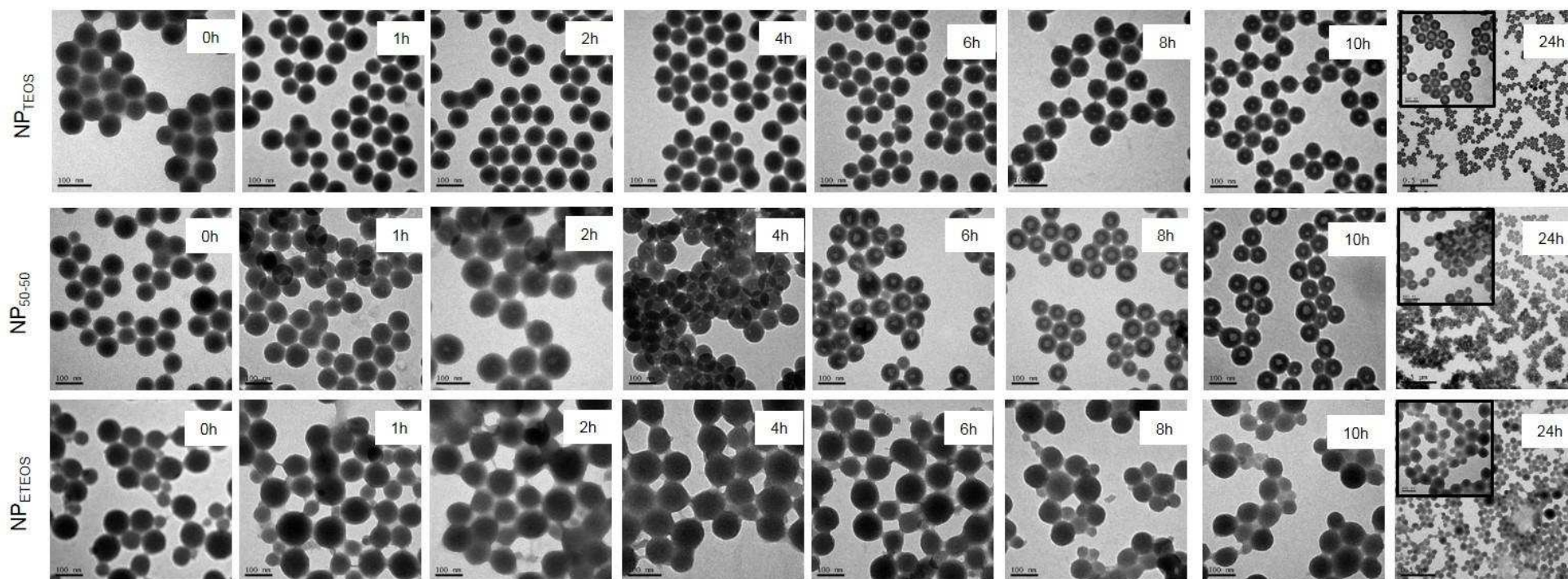


Figure S4: Degradation was visible by TEM for the three sets of NPs in pH 6 solution over time. Hollowing in the interior of NP_{TEOS} and NP₅₀₋₅₀ was observed after 6 – 8 hours whereas NP_{ETEOS} appeared to degrade at the particle surface.

pH 7.4

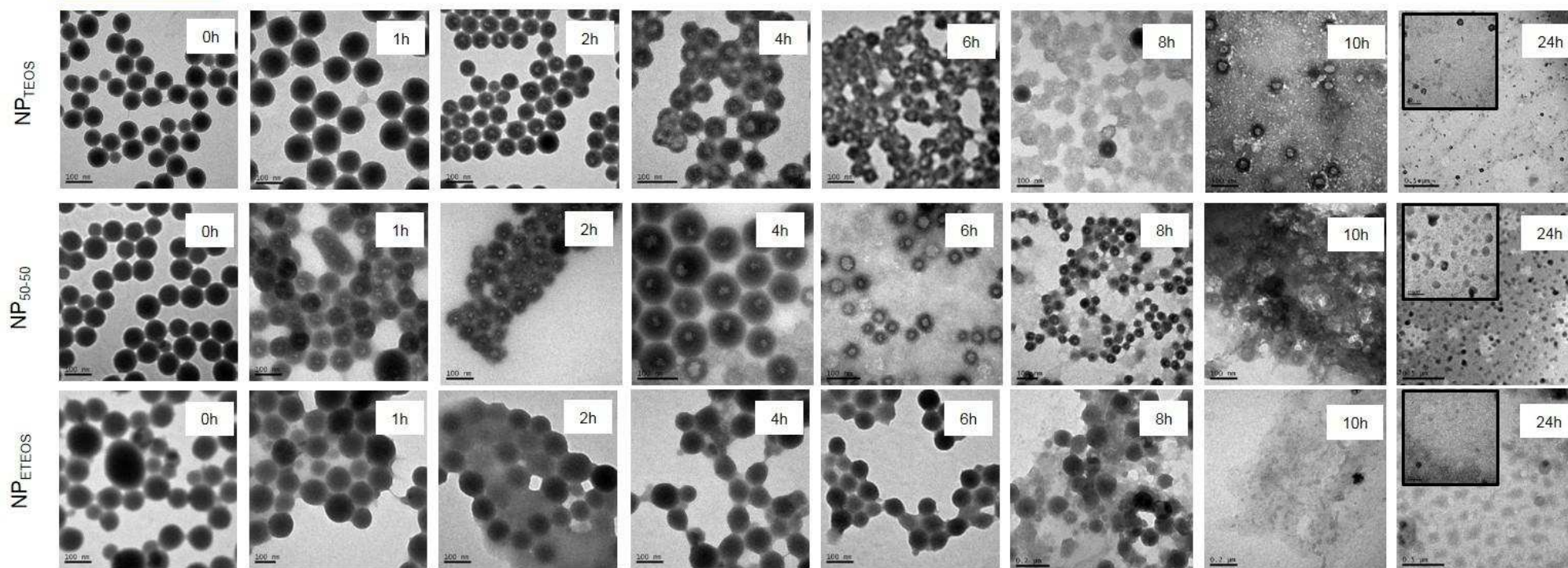
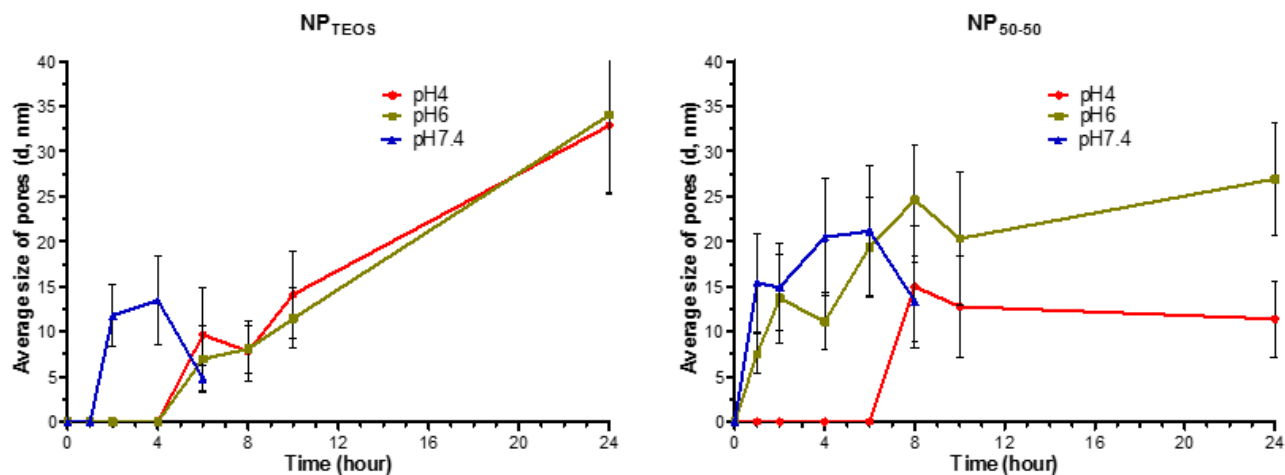
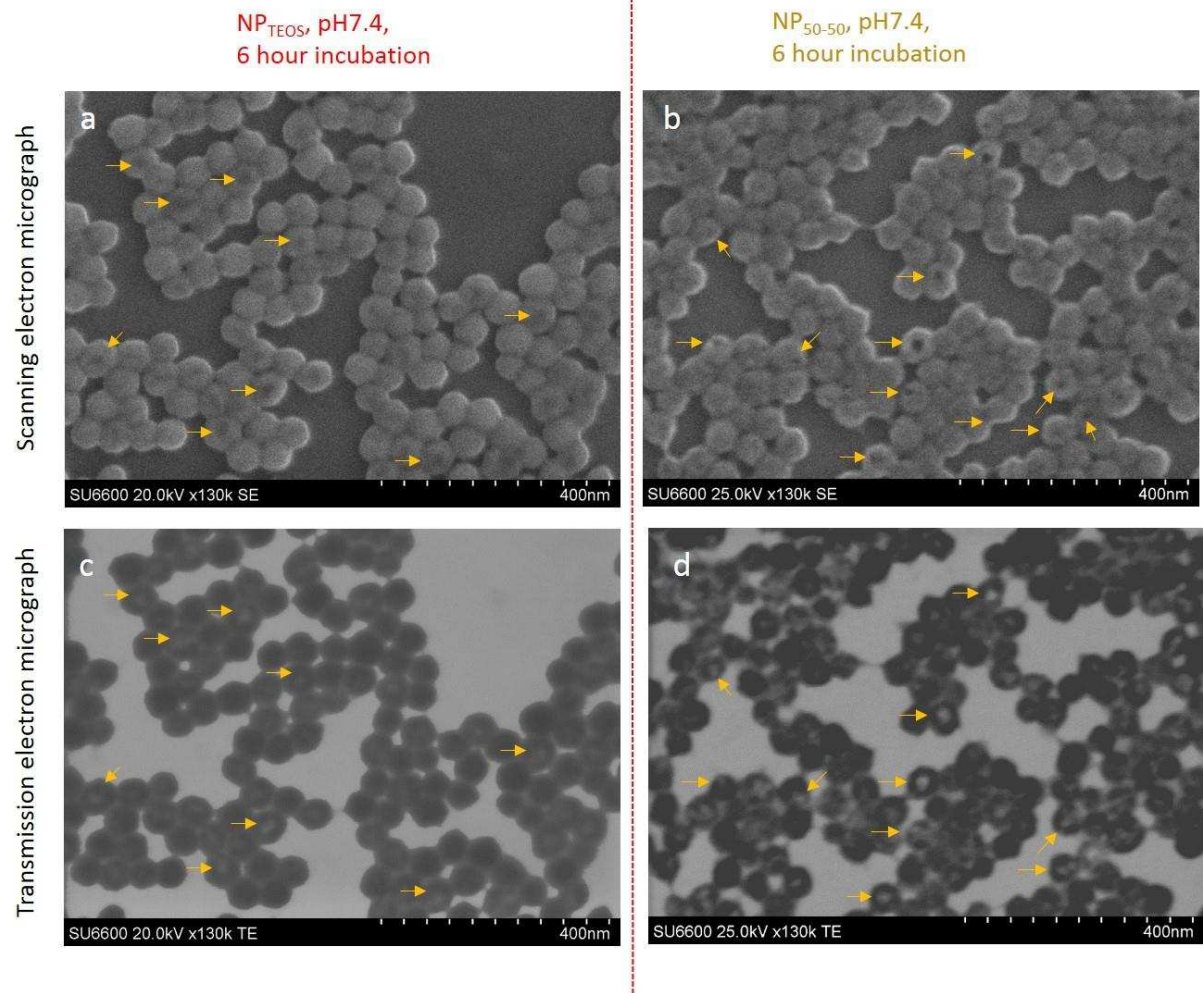


Figure S5: Degradation was visible by TEM for the three sets of NPs in pH 7.4 solution over time. More rapid hollowing of the interior of NP_{TEOS} and NP₅₀₋₅₀ was observed compared to those observed at pH 6. After 6 – 8 hours few NPs could be isolated after centrifugation and those after that time NP_{TEOS} appeared to degrade at the particle surface. After 10 hours virtually no NPs were visible by TEM, and structures resembling colloids were highly degraded and surrounded by dissolution debris.



		0h	1h	2h	4h	6h	8h	10h	24h
pH4	NP _{TEOS}	NM	NM	NM	NM	9.7±5.3	7.8±3.3	14.1±4.9	32.8±7.7
	NP ₅₀₋₅₀	NM	NM	NM	NM	NM	15.0±6.8	12.8±5.7	11.4±4.3
	NP _{ETOS}	NM	NM	NM	NM	NM	NM	NM	NM
pH6	NP _{TEOS}	NM	NM	NM	NM	7.0±3.7	8.1±2.6	11.5±3.4	34.0±8.7
	NP ₅₀₋₅₀	NM	7.5±2.2	13.7±4.9	11.1±3.2	16.4±5.5	24.6±6.2	20.3±7.3	26.9±6.2
	NP _{ETOS}	NM	NM	NM	NM	NM	NM	NM	NM
pH7.4	NP _{TEOS}	NM	NM	11.8±3.4	13.5±5.0	4.8±1.4	DISS.	DISS.	DISS.
	NP ₅₀₋₅₀	NM	15.4±5.4	14.9±4.8	20.5±6.5	21.2±7.2	13.4±4.4	DISS.	DISS.
	NP _{ETOS}	NM	NM	NM	NM	NM	NM	DISS.	DISS.

Figure S6: The size of the NP hollows (or pores) were measured by TEM analysis using the micrographs from Figures S3, S4 and S5. NM (not measurable) indicates that the particles did not present any visible pores, while DISS (dissolved) indicates that no particles were identifiable on the TEM grid and were therefore considered to be dissolved. Values are shown as average \pm SD (n=30 approximately).



*Figure S7: Scanning transmission electron microscopy allowed for secondary electrons (SE) to be obtained for scanning mode while transmission electrons (TE) could be detected simultaneously in transmission mode. **(a,b)** Scanning electron micrographs showed that the surface deformations, highlighted by yellow arrows, were visualised as hollows in transmission electron micrographs **(c,d)**. It is therefore suggested to that studies investigating silica NP hollowing/etching of the core should also use scanning electron microscopy to interrogate the particle surface, thus providing a more accurate evaluation of the overall particle morphology and integrity.*

